ACCEPTED FOR PUBLICATION IN PHYS. REV. B15

(1)

Infrared Properties of Pt/Al_2O_3 Cermet Films

M. F. MacMillan and R. P. Devaty

Department of Physics and Astronomy

100 Allen Hall

University of Pittsburgh

Pittsburgh, PA 15260

and

J. V. Mantese

Electrical and Electronics Engineering Department

General Motors Research Laboratories

Warren, MI 48090

ONR

PACS Numbers: 78.30.-j, 78.65.Pi, 42.20.Dd

N00014-85-K-0808

ABSTRACT

The room temperature transmittance and front reflectance of mid- and near-infrared radiation (400 - 15,000 cm^{-1}) by thin Pt/Al_2O_3 cermet films prepared by electron beam evaporation onto sapphire substrates were measured using a Fourier transform spectrometer. The high value of the dc percolation threshold f_c ($0.50 \leq f_c \leq 0.59$) for the Pt/Al_2O_3 system is evidence for correlations in the positions of the particles that can be described by coated-grain topologies. The data were compared with the predictions of five effective medium models, which feature different microstructural topologies.

and values of f_c. Published data on the dielectric functions of the component materials were used in the modeling. The Maxwell-Garnett and Bruggeman models do not describe the data adequately. A simplified version of a model by Sheng ($f_c \simeq 0.455$) provides an improved description. The best agreement is achieved for two models with adjustable, high values of f_c. We conclude that an effective medium theory is able to describe the infrared optical properties of a cermet system over a wide range of composition if proper account is taken of both the microstructure and the value of f_c.

I. INTRODUCTION

Effective medium theories[1] are commonly used to model the optical properties of granular composite materials such as cermet films[2-19]. If one considers a two-component metal-insulator composite material over the complete range of composition, a characteristic parameter relevant to both the electrical and optical properties is the percolation threshold, f_c. If f is the volume fraction of the metallic component imbedded in a perfectly insulating host, f_c indicates the onset of electrical conduction. Sufficiently close to f_c, the quasistatic approximation that underlies the effective medium approach breaks down because the mean cluster size exceeds the wavelength[20]. In this region of composition, recent theories based on scaling are applicable[20-26]. In this work, we do not focus on the region near f_c; rather, we are concerned with a broad range of composition. The role of the microstructure especially the topology of the material at the microscopic level, in determining the effective optical properties of composite materials has been demonstrated[2,12]. For example, Gibson, *et al.*[2], applied a simplified version of a model introduced by Sheng[27], which was based on ideas concerning the growth of cermet films, to successfully account for the optical properties of their samples.

In this paper, we present room temperature transmittance and reflectance data on thin granular Pt/Al_2O_3 cermet films that were deposited on crystalline sapphire substrates. The set of samples covers a broad range of composition. This system possesses a relatively high value of f_c, which is indicative of a coated grain topology. The data are compared with five effective medium theories that describe different microstructural morphologies and feature different values of f_c. Published optical data on the component materials are used in the modeling. The best agreement between theory and experiment is provided by theories with adjustable high values of f_c. The differences in predicted optical properties of effective medium theories with the same f_c are associated with the microstructure.

Section II discusses the effective medium theories used in this paper. The Maxwell-Garnett[28],

Bruggeman[29], and Sheng[27] effective medium theories are reviewed. Two effective medium theories with adjustable values of f_c are introduced. The value of f_c is set by specifying composition dependent fractions for the basic cells that describe the microscopic topology of the medium. One of these models is based on the model of Mantese, *et al.*[30], for the dc conductivity of the same Pt/Al_2O_3 films under consideration here. The other model represents a different microstructural topology. The effects of particle correlations are included in both models. The effective medium theories are compared for the case of the frequency dependence of the imaginary part of the effective dielectric function for a Drude metal in a perfect insulator. The effecive medium theories that are based on rather complex basic cells predict a plethora of structure in the optical properties. Section III discusses the experimental work. A brief account given earlier[31]. Section IV contains the comparison between the five effective medium theories and the data. Section V summarizes the results.

II. THEORY

In the effective medium approach, the microscopically inhomogeneous composite material is modeled by a complex frequency dependent homogeneous dielectric function. This approach is valid if the quasistatic approximation applies; i.e., if the wavelength of the electromagnetic radiation in all of the component materials is much greater than the grain sizes and cluster sizes. The results of electrostatics are used to match the fields at the boundaries. A set of basic unit cells, usually with spherical symmetry, is chosen based on the microstructure of the composite material. Self consistency is achieved[32] by demanding that there be no additional scattering when the basic cells are imbedded in the effective medium. For spheres in three dimensions, this condition is

$$\sum_{i=1}^{N} \frac{p_i(\epsilon_i - \tilde{\epsilon})}{\epsilon_i + 2\tilde{\epsilon}} = 0, \tag{1}$$

where p_i is the probability that a cell is of the ith type, ϵ_i is its effective dielectric function, $\bar{\epsilon}=\bar{\epsilon}'+i\bar{\epsilon}''$ is the complex frequency dependent dielectric function of the effective medium, and N is the number of distinct basic cells. In general, p_i can depend on the composition. For example, for a two-component metal-insulator composite with metallic volume fraction f, $p_i=p_i(f)$. The choice of basic cells should be based on an understanding of the microstructural morphology of the composite material. The importance of microstructure in determining the effective optical constants of composite materials has been demonstrated experimentally[2,12]. In addition, it is thought that the region of the complex plane accessible to $\bar{\epsilon}$ by the Milton-Bergman bounds[33-34] is related to the possible microstructures[34].

In this section we discuss the five effective medium theories that we later compare with our data on Pt/Al_2O_3 cermet films. The associated basic cells are shown schematically in Figure 1. Note that the number of basic cells need not be the same as the number of component materials. For each model, we discuss the behavior of $\bar{\epsilon}''(\omega;f)$, the dissipative part of $\bar{\epsilon}$, for a two-component composite material consisting of Drude metal imbedded in an insulating host. The Drude dielectric function is

$$\epsilon_m(\omega) = \epsilon_l\left(1+\frac{i\omega_p^2\tau}{\omega(1-i\omega\tau)}\right), \tag{2}$$

where ω is the circular frequency, ω_p is the plasma frequency, τ is the relaxation time, and ϵ_l takes core polarization into account. For the calculations, we choose $\tilde{\omega}_p=10{,}000\ cm^{-1}$ ($\tilde{\omega}=\omega/2\pi c$ is the frequency in wavenumbers), $(2\pi c\tau)^{-1}=10\ cm^{-1}$, and $\epsilon_l=1$. For the insulating host, $\epsilon_h=2.0$. Although the optical properties of the component materials are simple, surprisingly complex structure is predicted by some of the effective medium theories.

A. Maxwell-Garnett Model

The Maxwell-Garnett[28] (MG) effective dielectric function can be obtained by inserting the

dielectric function for a dielectric-coated metal sphere[35], ϵ_c, into Eq. 1. The result is

$$\bar{\epsilon} = \epsilon_c = \epsilon_h \frac{2(1-f)\epsilon_h + (1+2f)\epsilon_m}{(2+f)\epsilon_h + (1-f)\epsilon_m}. \tag{4}$$

There is no percolation threshold associated with this model, due to the coated metallic grain topology. For the MG model to apply to a composite with large metallic content, it is clear that the particles must be highly correlated. Fig. 2 shows $\bar{\epsilon}''(\omega;f)$. The sharp plasma resonance, with frequency $\omega_1 = \sqrt{\epsilon_l/(2\epsilon_h+\epsilon_l)}\omega_p$ in the low f limit, shows a redshift and broadens with increasing f. One can also derive a reversed MG model based on a metal-coated dielectric sphere as the basic cell.

B. Bruggeman Model

The Bruggeman model[29], sometimes called "the effective medium theory," is obtained by choosing spherical basic cells of each component material for Eq. 1. The quadratic equation

$$\frac{f(\epsilon_m - \bar{\epsilon})}{\epsilon_m + 2\bar{\epsilon}} + \frac{(1-f)(\epsilon_h - \bar{\epsilon})}{\epsilon_h + 2\bar{\epsilon}} = 0 \tag{5}$$

must be solved. The correct solution is the one with positive $\bar{\epsilon}''$, corresponding to dissipation. Eq. 5 is symmetric in the component materials. The percolation threshold is $f_c = \frac{1}{3}$. Figure 3 shows that the sphere resonance associated with an isolated metallic particle is broadened into an "impurity band[36]" even at low f. This band broadens and its peak is redshifted with increasing f. A nonzero value of $\bar{\epsilon}''$ at zero frequency associated with nonzero dc electrical conductivity is obtained for $f > f_c$. Above f_c, the "impurity band" narrows and approaches the frequency of the dielectric "void" resonance, $\omega_2 = \sqrt{2\epsilon_l/(2\epsilon_l+\epsilon_1)}\omega_p$, corresponding to a dielectric surrounded by metal, as f approaches unity.

C. Sheng Model

Sheng[27] introduced a probabilistic growth model for cermet films. We make use of a simplified version of the model that was introduced by Gibson, *et al.*[2]. The basic cells are dielectric-coated metal (ϵ_1) and metal-coated dielectric (ϵ_2) spheres, each having the composition of the composite material. The dielectric function is obtained by solving

$$\frac{p_1(\epsilon_1-\bar{\epsilon})}{\epsilon_1+2\bar{\epsilon}} + \frac{p_2(\epsilon_2-\bar{\epsilon})1}{\epsilon_2+2\bar{\epsilon}} = 0, \tag{6}$$

where ϵ_1 and ϵ_2 are identical to $\bar{\epsilon}$ for the MG model and reversed MG model, respectively. The probabilities p_1 and p_2 are determined by a free volume argument. p_1 is proportional to the number of possible configurations of a metal sphere of radius r within a larger dielectric sphere of radius R. Assuming that all configurations are equally probable, $p_1 \sim (1-r/R)^3$. Since $f=(r/R)^3$,

$$p_1 = \frac{(1-f^{1/3})^3}{[(1-f^{1/3})^3 + (1-(1-f)^{1/3})^3]} \tag{7}$$

and $p_2=1-p_1$. The percolation threshold is obtained from the equation for the effective dc conductivity,

$$\frac{p_1(\sigma_1-\bar{\sigma})}{\sigma_1+2\bar{\sigma}} + \frac{p_2(\sigma_2-\bar{\sigma})}{\sigma_2+2\bar{\sigma}} = 0. \tag{8}$$

Since $\sigma_1=0$, we obtain $\bar{\sigma}=0$ for $f<f_c$ and

$$\bar{\sigma} = (1-\tfrac{3}{2}p_1)\sigma_2 \tag{9}$$

for $f > f_c$. Setting $\bar{\sigma} = 0$ in Eq. 9, we obtain

$$p_1(f_c) = \frac{2}{3}. \tag{10}$$

The result is $f_c \simeq 0.455$ in three dimensions[37].

The rather complex structure in the optical properties of a composite material predicted by this model is illustrated in Fig. 4. At low f, we see the sphere resonance associated with the dielectric-coated metal sphere, which dominates at low f. The plot for f=.20 shows additional resonances, near $\omega = 0$ and $\omega = \omega_p$. These resonances are associated with the metal-coated dielectric sphere, imbedded in an insulating effective medium ($f < f_c$). The "impurity band" structure at intermediate compositions is far more complex here, so that it is difficult to interpret in detail. The appearance of a peak at zero frequency corresponds to the onset of dc conduction. At large f (near 1), the dielectric void resonance associated with the metal-coated dielectric sphere appears. To the best of our knowledge, most of the predicted structure in the optical properties has not yet been observed experimentally.

D. Modified Mantese-Curtin-Webb Model

Mantese, *et al.*[30], introduced a model for the composition dependence of the room temperature dc resistivity of Pt/Al_2O_3 cermet films from the set of samples under study here. The model includes the contribution of interparticle tunneling, and a principal conclusion of their paper is that tunneling is required to explain the measured dc electrical conductivity and noise. It is also important that correlations between the particles are included. This model is not easily generalized to finite frequencies.

We introduce a model with a similar microstructure and the same composition dependence for the probability distribution of the basic cells. Mantese, *et al.*, chose $p(f) = f^2$ for the fraction of

conducting cells in a film with metallic volume fraction f. Note that the basic cells and their probability distributions may be independently specified. We choose the basic cells of the simplified Sheng model, but use $p_2(f)=f^2$. The percolation threshold obtained from Eq. 10 is $f_c=1/\sqrt{3}\simeq 0.577$.

Figure 5 shows the frequency and composition dependence of $\bar{\epsilon}''$ for this model. Not surprisingly, the qualitative behavior is similar to the Sheng model.

E. Effective Medium with Correlated Particles

We have seen that it is important to consider both the microstructure and the value of f_c when constructing an effective medium theory. For the samples under consideration, the measured percolation threshold is high[30] ($0.5\leq f_c\leq .59$), so that the particles are correlated. We introduce a new effective medium theory with a different microstructure than those discussed above.

The percolation thresholds of the BR and Sheng models are too low for the present application. We introduce correlations by adding to the basic cells of the BR model a dielectric coated sphere (See Fig. 1). The metallic fraction in the coated sphere is f, the volume fraction in the material as a whole. The new model is asymmetric in the components, but apparently so is the Pt/Al_2O_3 system. The percolation threshold can be varied over $1/3\leq f_c\leq 1$ through the choice of the probability distributions. We note that a similar effective medium theory with low percolation thresholds ($0\leq f_c\leq 1/3$) can be constructed by choosing a metal-coated dielectric sphere. The dielectric function for this Correlated Effective Medium Theory (CEMT) is determined by solving

$$\frac{(1-p)\,f\,(\epsilon_m-\bar{\epsilon})}{\epsilon_m+2\bar{\epsilon}}+\frac{(1-p)(1-f)(\epsilon_h-\bar{\epsilon})}{\epsilon_h+2\bar{\epsilon}}+\frac{p(\epsilon_c-\bar{\epsilon})}{\epsilon_c+2\bar{\epsilon}}=0. \qquad (11)$$

The function p(f) is chosen by ansatz. We choose $p(f)=\cos^a(\pi f/2)$, where a is an adjustable parameter. This function obeys $p(0)=1$ and $p(1)=0$. The first condition states that the entire

medium has the coated grain topology, like the MG model, at f=0. The latter condition is required so that the dc conductivity approaches the bulk value continuously as f approaches unity.

The percolation threshold is determined by solving the equation for the effective conductivity, similar to Equation 11, under the condition $\sigma_h = \sigma_c = 0$. The resulting condition is

$$1 - 3[1-p(f_c)]\, f_c = 0. \tag{12}$$

For our chosen distribution,

$$a = \frac{\ln(1-1/3f_c)}{\ln(\cos(\pi f_c/2))}. \tag{13}$$

We choose $f_c = 1/\sqrt{3}$, for comparison with the modified model of Mantese, *et al.* Thus, $a \simeq 1.78$.

Figure 6 shows $\tilde{\epsilon}''$ for the CEMT. The sharp sphere resonance is observed at small f. At intermediate f, rather complex behavior associated with "impurity bands" is observed. Near f=1, the band associated with the dielectric void resonance is observed.

III. EXPERIMENT

The Pt/Al_2O_3 granular films[38] were prepared by coevaporation of Pt and Al_2O_3 onto single crystal sapphire wafers in a dual e-beam evaporator with a low base pressure (mid 10^{-7} torr). The volume fraction of Pt in the films, which ranges from 0.23 to 1.00, was determined by monitoring the relative deposition rates of the two materials using quartz crystal oscillators inside the evaporation chamber. The film thicknesses, which were measured with a Dektak surface profilometer, ranged from 1100 Å to 2100 Å. The orientations of the sapphire substrates, as determined by back reflection Laue photographs, were about 20° from the ordinary axis. The percolation threshold, as determined by the

temperature dependence of the dc resistivity, was in the range of 50-59% Pt by volume[39]. Although no direct determination of the microstructure by electron microscopy has been performed on these films, the high value of f_c is a strong indicator of a coated grain topology. Electron micrographs on cermet films prepared by the same method support this conclusion[39-40].

The room temperature transmittance and relative reflectance data were measured using a Nicolet 740 Fourier transform infrared spectrometer under a nitrogen purge. The spectral range $400-15{,}000\ cm^{-1}$ was covered using three combinations of sources, beamsplitters, and detectors. The range $400-5{,}000\ cm^{-1}$ was covered using a glowbar source, KBr beamsplitter, and DTGS detector. The near infrared was covered using a tungsten lamp, solid quartz beamsplitter, and room temperature PbSe ($5{,}000-11{,}000\ cm^{-1}$) and Si diode ($11{,}000$-$15{,}000\ cm^{-1}$) detectors. The resolution was $4\ cm^{-1}$ for all three regions. For the transmittance measurements, the "sample in−sample" out method was used. For the reflectance measurements, the samples were mounted on a Spectra Tech Model 500 variable angle specular reflectometer. The angle of incidence was set at 5° from the normal. A 100% Pt film from the set of samples was used as the reflectance reference. The reflectance, as displayed in the figures, was obtained by multiplying the reflection ratio by interpolations of tabulated values[41] of the reflectance of Pt. Thus, we have an estimate of the absolute reflectance of the sample.

The dependence of the transmittance and reflectance of the f=0.23 sample on the angle of rotation about the beam axis were measured to determine if the optical anisotropy of the sapphire substrate affects the results. The transmittance varies by about 3−4% as the sample is rotated through 360° in 15° increments. The reflectance measurements show no such effect. The orientational dependence of transmittance and reflectance was also studied with the sample placed between crossed polarizers[42]. Four maxima in transmittance were observed for a 360° rotation.

Yariv and Yeh[43] treat the problem of transmission through an anisotropic material between crossed polarizers using Jones calculus. The transmitted intensity is

$$I(\psi,\gamma) = \frac{1}{2}\sin^2\left(\frac{\gamma}{2}\right)\sin^2(2\psi). \qquad (14)$$

Here ψ is the angle of rotation about the beam axis and $\gamma = (n_o - n_e(\theta))\, d\tilde{\omega}$, where n_o and $n_e(\theta)$ are the ordinary and extraordinary indices of refraction, respectively, θ is the angle between the beam and the symmetry axis of the uniaxial crystal, d is the substrate thickness, and $\tilde{\omega}$ is the frequency in wavenumbers. Eq. 14 predicts four maxima, in agreement with experiment. We conclude that substrate anisotropy is a sufficiently important effect that we cannot reliably convert our data into optical constants. Thus, we compare the measured transmittance and reflectance directly with computed spectra.

IV. RESULTS AND DISCUSSION

We test the five effective medium models by direct comparison with the measured transmittance and reflectance of Pt/Al_2O_3 films covering a broad range of composition. Theoretical expressions for the transmittance and reflectance are obtained using the matrix method[44] for absorbing films on an absorbing substrate. Interference effects are included for the film but neglected for the substrate. In the course of this work, we rediscovered an interesting interference effect that takes place when an electromagnetic wave propagating in an absorbing medium is incident on an interface[45]. Due to this effect, the sum of the transmittance and reflectance, calculated by ratios of Poynting vectors in the usual fashion do not sum to unity. Of course, when one examines the situation in detail, there is no violation of conservation of energy.

The calculations require knowledge of the bulk dielectric functions of the component materials, perhaps modified to account for size-induced effects. For Pt, Weaver's data[41] were used down to 806 cm^{-1}. A Drude model extrapolation was used for lower frequencies[46]. The properties of granular

Al_2O_3 host material have been measured by Eriksson, *et al*[17]. The optical properties of the crystalline sapphire substrates are based on an oscillator fit to measured data by Barker[18].

Figure 7 shows the measured transmittance for those films in the sample set that transmit infrared radiation and the predictions of the five effective medium theories. The noise in the data in the middle frequency region is due to the weakness of the signal, which was attenuated severely to minimize nonlinearity in the PbSe detector response. Some sharp lines due to atmospheric absorption not entirely eliminated by purging are also evident. The step near 10,000 cm^{-1} is an artifact due to the change in detectors. It is clear that Maxwell-Garnett and Bruggeman models do not provide a good description of our data. The roles of microstructural topology and values of f_c are important. The MG model predicts too much transmission, especially at high f, because there is no percolation. The BR model predicts insufficient transmission, since f_c is too low. The Sheng model does a better job, but the two models with adjustable, and hence high, f_c are best. We feel that the details of the transmission, as well as the magnitude, are best described by the CEMT, although the modified model of Mantese *et al.*[30] is almost as good.

Figures 8 and 9 provide comparisons of the measured reflectance with the predictions of the effective medium theories for a wide range of composition. Over the complete range of infrared frequencies, the two effective medium theories with large f_c that include the effect of correlations provide the best description, with a slight edge to the CEMT. Note that the details of optical structure discussed for a simple Drude metal imbedded in a nonabsorbing host are not observed. Pt is certainly not a Drude metal, and the frequency region covered does not include the entire interesting region in Pt. Figure 9 shows the low frequency reflectance, where details of optic phonons of the host material and crystalline sapphire substrate are evident. Notice that the structure due to the optic phonons is masked for concentrations near and above the percolation threshold, since the conductive properties of the film dominate. The percolation threshold estimated by this optical method agrees with the dc

value.

Figure 10 shows the volume fraction dependence of the absorptance (1−R−T) for selected infrared frequencies. There is an anomalous peak in the measured absorptance near the percolation threshold. Such absorption has been identified in previous experiments[49]. The peak broadens and shifts to lower volume fractions with increasing frequency. The CEMT once again provides the best description of the complete data set.

Robin and Souillard[24-25] have developed a model for the anomalous absorption in the infrared properties of granular metal films based on scaling ideas. The absorption is associated with the large clusters of metal particles that exist near p_c. They predict that the width of the region of anomalous absorption behaves as $\delta f \sim (\lambda/2\pi a)^{-1/\nu}$, where λ is the wavelength, a the particle size, and ν the exponent associated with the percolation correlation length[50]. This model correctly predicts the increase in width with frequency, at least qualitatively.

V. CONCLUSION

We have compared the measured transmittance and reflectance of Pt/Al_2O_3 films covering a broad range of composition with the predictions of effective medium theories and the measured optical properties of the bulk component materials. We conclude that the effective medium approach provides an good description for our system, which shows a relatively high percolation threshold, if the theoretical f_c is adjusted to the measured value and the effective medium theory has the appropriate microstructural topology. We conclude that the correlations between particles make an important contribution to the optical properties in this system. Future work on cermet films should include a detailed examination of the behavior very close to f_c to further test recent theoretical progress based on scaling theory. Refinements in techniques of sample preparation will be required to precisely control both the composition and microstructure.

ACKOWLEDGEMENTS

This work was supported by the Office of Naval Research Contract N00014-85-K-0808.

REFERENCES

1. R. Landauer, in Electrical Transport and Optical Properties of Inhomogeneous Media—1977, J. C. Garland and D. B. Tanner, eds., AIP Conf. Proc. No. 40 (American Institute of Physics, New York, 1977), p. 2.
2. U. J. Gibson, H. G. Craighead, and R. A. Buhrman, Phys. Rev. B25, 1449 (1982).
3. R. W. Cohen, G. D. Cody, M. D. Coutts, and B. Abeles, Phys. Rev. B8, 3689 (1973).
4. J. C. C. Fan and P. M. Zavracky, Appl. Phys. Lett. 29, 478 (1976).
5. J. I. Gittleman, B. Abeles, P. Zanzucchi, and Y. Arie, Thin Solid Films 45, 9 (1977).
6. C. G. Granqvist, J. Appl. Phys. 50, 2916 (1979).
7. G. A. Niklasson, C. G. Granqvist, and O. Hunderi, Appl. Opt. 20, 26 (1981).
8. G. A. Niklasson and C. G. Granqvist, J. Appl. Phys. 55, 3382 (1984).
9. T. Yamaguchi, M. Sakai, and N. Saito, Phys. Rev. B32, 2126 (1985).
10. D. Evans, Phys. Rev. B32, 4169 (1985).
11. T. W. Noh, Y. Song, S.-I. Lee, J. R. Gaines, H. D. Park, and E. R. Kreidler, Phys. Rev. B33, 3793 (1986).
12. D. E. Aspnes, Phys. Rev. B33, 677 (1986).
13. S. Berthier and J. Lafait, Thin Solid Films 89, 213 (1982).
14. S. Berthier, J. Lafait, C. Sella, and T. K. Vien, Thin Solid Films 125, 171 (1985).
15. S. Berthier and J. Lafait, J. Phys. (Paris) 47, 249 (1986).
16. J. Lafait, S. Berthier, C. Sella, and T. K. Vien, Vacuum 36, 125 (1986).

17. S. Berthier, K. Driss-Khodja, and J. Lafait, J. Phys. (Paris) 48, 601 (1987).

18. M. Gadenne, J. Lafait, and P. Gadenne, Physica A157, 400 (1989).

19. M. Gajdardziska-Josifovska, R. C. McPhedran, D. R. McKenzie, and R. E. Collins, Appl. Opt. 28, 2744 (1989).

20. Y. Yagil and G. Deutscher, Appl. Phys. Lett. 52, 373 (1988),

21. A. I. Efros and B. I. Shklovskii, Phys. Stat. Sol. (b) 76, 475 (1976).

22. D. J. Bergman and Y. Imry, Phys. Rev. Lett. 39, 1222 (1977).

23. D. Stroud and D. J. Bergman, Phys. Rev. B25, 2061 (1982).

24. Th. Robin and B. Souillard, Europhys. Lett. 8, 753 (1989).

25. Th. Robin and B. Souillard, Physica A157, 285 (1989).

26. Th. Robin and B. Souillard, Opt. Commun. 71, 15 (1989).

27. P. Sheng, Phys. Rev. Lett. 45, 60 (1980).

28. J. C. M. Garnett, Phil. Trans. R. Soc. London Ser. A 203, 385 (1904); 205, 237 (1906).

29. D. A. G. Bruggeman, Ann. Phys. (Leipzig) 24, 636 (1935).

30. J. V. Mantese, W. A. Curtin, and W. W. Webb, Phys. Rev. B33, 9897 (1986).

31. M. F. MacMillan, R. P. Devaty, and J. V. Mantese, Mat. Res. Soc. Symp. Proc. Vol. 132, 99 (1989).

32. D. Stroud and F. P. Pan, Phys. Rev. B17, 1602 (1978).

33. D. J. Bergman, Ann. Phys. (New York) 138, 78 (1982).

34. G. W. Milton, J. Appl. Phys. 52, 5286 (1981).

35. H. C. van de Hulst, Light Scattering by Small Particles (Dover, New York, 1981), pp. 73-74.

36. D. Stroud, Phys. Rev. B19, 1783 (1979).

37. f_c for the simplified Sheng model is given incorrectly in references 2 and 31.

38. J. V. Mantese, Ph.D. Thesis, Cornell University (1985).

39. H. G. Craighead, Ph.D. Thesis, Cornell University (1980).

40. U. J. Gibson, Ph.D. Thesis, Cornell University (1982).

41. D. W. Lynch and W. R. Hunter, in Handbook of Optical Constants of Solids, edited by E. Palik (Academic Press, New York, 1985).

42. Molectron Detector, Inc., $8-12$ μm thin film grid polarizers on BaF_2 substrates.

43. A. Yariv and P. Yeh, Optical Waves in Crystals (Wiley, New York, 1984).

44. O. S. Heavens, Optical Properties of Thin Solid Films (Butterworth Publications, Ltd., London, 1955).

45. Z. Knittl, Optics of Thin Films (Wiley, New York, 1976), and references therein.

46. M. A. Ordal, R. J. Bell, R. W. Alexander, Jr., L. L. Long, and M. R. Querry, Appl. Opt. 24, 4493 (1985).

47. T. S. Eriksson, A. Hjortsberg, G. A. Niklasson, and C. G. Granqvist, Appl. Opt. 20, 2742 (1981).

48. A. S. Barker, Jr., Phys. Rev. 132, 1474 (1963).

49. P. Gadenne, Y. Yagil, and G. Deutscher, J. Appl. Phys. 66, 3019 (1989); Physica A157, 279 (1989).

50. D. Stauffer, Introduction to Percolation Theory (Taylor and Francis, London, 1985).

FIGURE CAPTIONS

Figure 1. Schematic of self-consistent imbedding of basic unit cells associated with the five effective medium models. The darkly shaded regions represent metal, the unshaded regions insulator, and the lightly shaded regions the homogeneous effective medium. The microscopic topologies are associated with the following models: a) Maxwell-Garnett, b) Bruggeman, c) Sheng and modified model of Mantese, *et al.*, and d) CEMT.

Figure 2. Frequency and volume fraction dependence of the imaginary part of the effective dielectric function for a two-component metal-insulator composite predicted by the Maxwell-Garnett model. The dielectric function of the metal is given by the Drude model with $\omega_p = 10{,}000$ cm^{-1}, $(2\pi c\tau)^{-1} = 10$ cm^{-1}, and $\epsilon_l = 1.0$. The insulating component is a perfect dielectric with $\epsilon_h = 2.0$.

Figure 3. Frequency and volume fraction dependence of the imaginary part of the effective dielectric function for a two-component metal-insulator composite predicted by the Bruggeman model. The dielectric function of the metal is given by the Drude model with $\omega_p = 10{,}000$ cm^{-1}, $(2\pi c\tau)^{-1} = 10$ cm^{-1}, and $\epsilon_l = 1.0$. The insulating component is a perfect dielectric with $\epsilon_h = 2.0$.

Figure 4. Frequency and volume fraction dependence of the imaginary part of the effective dielectric function for a two-component metal-insulator composite predicted by the Sheng model. The dielectric function of the metal is given by the Drude model with $\omega_p = 10{,}000$ cm^{-1}, $(2\pi c\tau)^{-1} = 10$ cm^{-1}, and $\epsilon_l = 1.0$. The insulating component is a perfect dielectric with $\epsilon_h = 2.0$.

Figure 5. Frequency and volume fraction dependence of the imaginary part of the effective dielectric function for a two-component metal-insulator composite predicted by the modified model of Mantese, *et al.* The dielectric function of the metal is given by the Drude model with $\omega_p = 10{,}000\ \mathrm{cm}^{-1}$, $(2\pi c\tau)^{-1} = 10\ \mathrm{cm}^{-1}$, and $\epsilon_l = 1.0$. The insulating component is a perfect dielectric with $\epsilon_h = 2.0$.

Figure 6. Frequency and volume fraction dependence of the imaginary part of the effective dielectric function for a two-component metal-insulator composite predicted by the CEMT. The dielectric function of the metal is given by the Drude model with $\omega_p = 10{,}000\ \mathrm{cm}^{-1}$, $(2\pi c\tau)^{-1} = 10\ \mathrm{cm}^{-1}$, and $\epsilon_l = 1.0$. The insulating component is a perfect dielectric with $\epsilon_h = 2.0$.

Figure 7. Comparison of measured transmittance of Pt/Al_2O_3 films with the predictions of effective medium theories. a) Data. b) CEMT. c) modified model of Mantese, *et al.* d) Sheng model. e) Bruggeman model. f) Maxwell-Garnett model. For the calculated spectra the line types denote volume fractions as follows: (———) f=0.23, (····) f=0.33, (–·–·) f=0.42, (----) f=0.50, (– – –) f=0.58, (–···–···) f=0.71, and (-–-–) f=0.83.

Figure 8. Comparison of measured reflectance of Pt/Al_2O_3 films with the predictions of effective medium theories. a) Data. b) CEMT. c) modified model of Mantese, *et al.* d) Sheng model. e) Bruggeman model. f) Maxwell-Garnett model. For the calculated spectra the line types denote volume fractions as follows: (———) f=0.23, (····) f=0.33, (–·–·) f=0.42, (----) f=0.50, (– – –) f=0.58, (–···–···) f=0.71, and (-–-–) f=0.83.

Figure 9. Comparison of measured low frequency reflectance of Pt/Al_2O_3 films with the predictions of effective medium theories. a) Data. b) CEMT. c) modified model of Mantese, *et al.* d) Sheng model. e) Bruggeman model. f) Maxwell-Garnett model. For the calculated spectra the line types denote volume fractions as follows: (———) f=0.23, ($\cdots$) f=0.33, ($-\cdot-\cdot$) f=0.42, (----) f=0.50, ($--$) f=0.58, ($-\cdots-\cdots$) f=0.71, and ($\cdot--\cdot--$) f=0.83.

Figure 10. Comparison of the Pt volume fraction dependence of the measured absorptance of Pt/Al_2O_3 films with the predictions of effective medium theories. a) data, b) CEMT, c) modified model of Mantese, *et al.*, d) Sheng model, e) Bruggeman model, and f) Maxwell-Garnett model. The line types denote frequencies as follows: (———) 4,000 cm^{-1}, ($\cdots$) 6,000 cm^{-1}, ($\cdot-\cdot-$) 8,000 cm^{-1}, (----) 10,000 cm^{-1}, ($--$) 12,000 cm^{-1}, and ($\cdots-\cdots-$) 14,000 cm^{-1}.

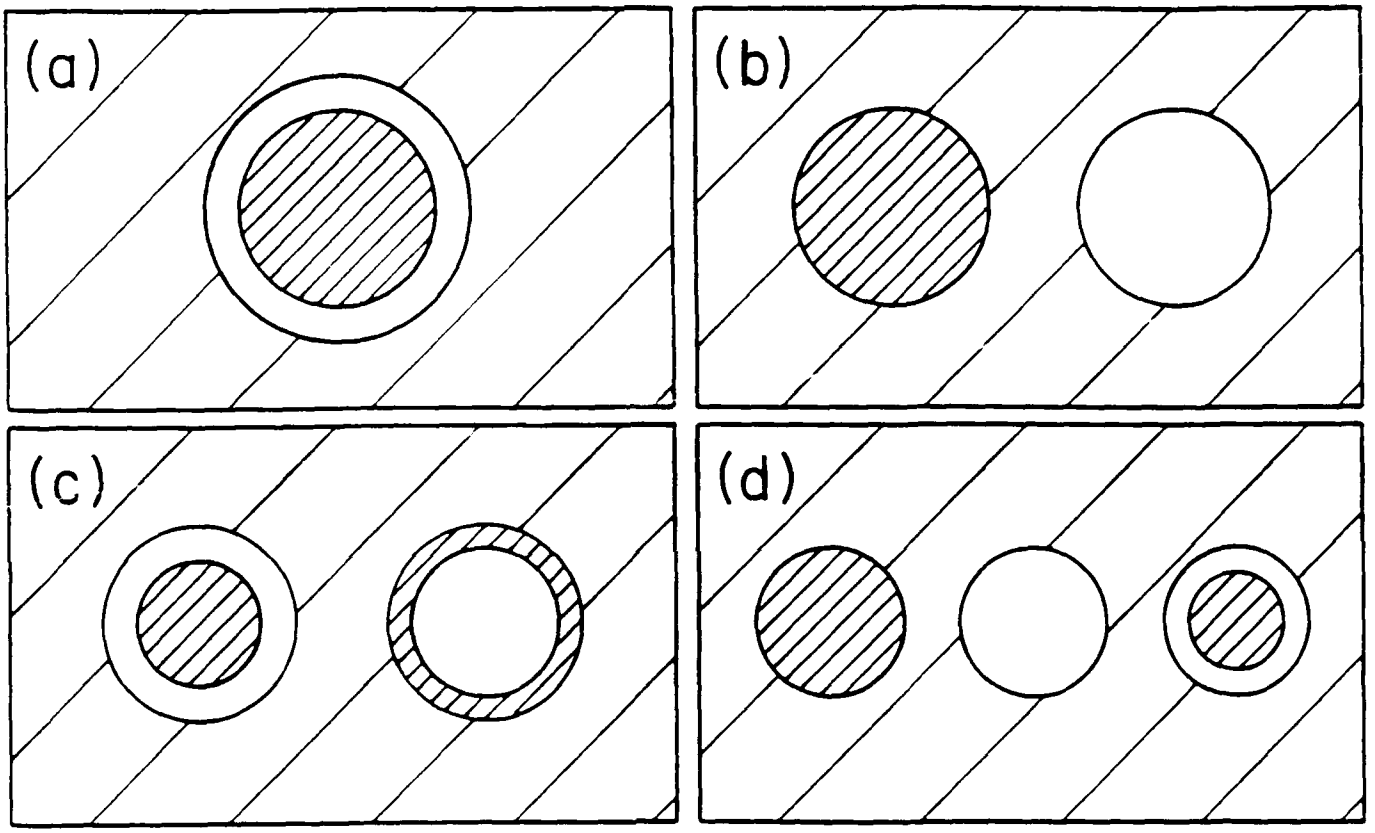
(a)
(b)
(c)
(d)

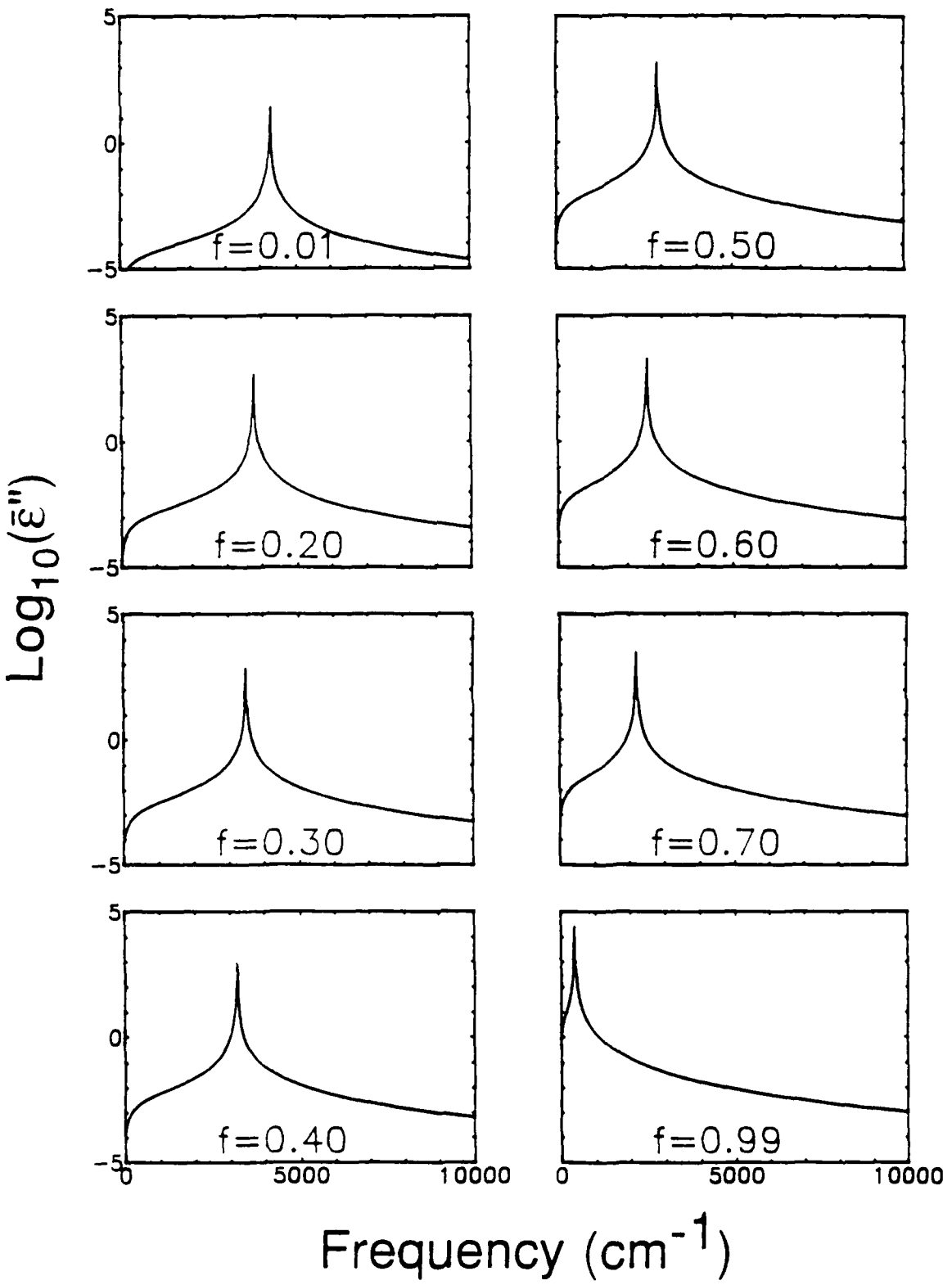

MACMILLAN, DEVATY, + MANTESE FIG. 2

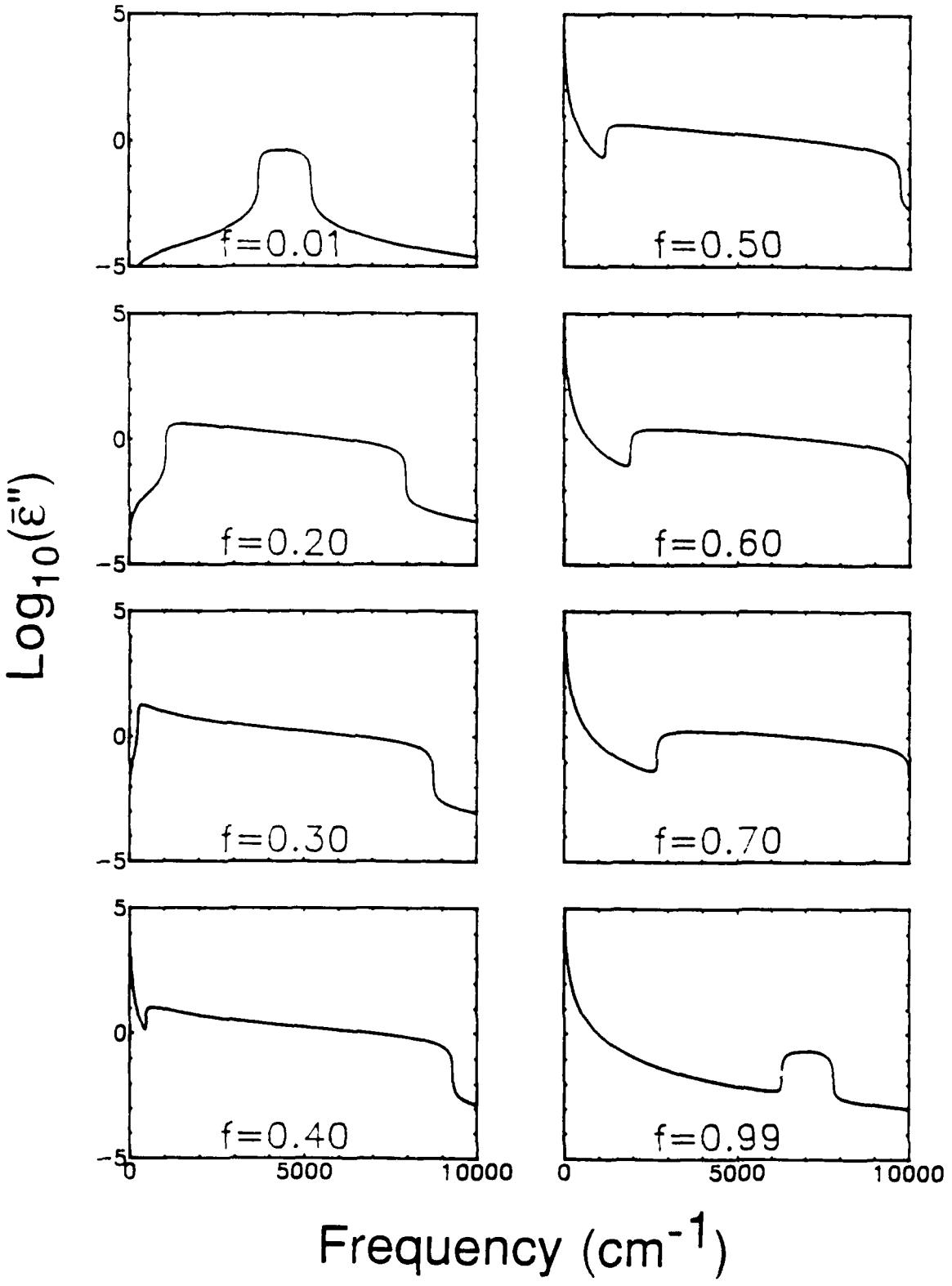

MacMILLAN, DEVATY, + MANTESE FIG. 3

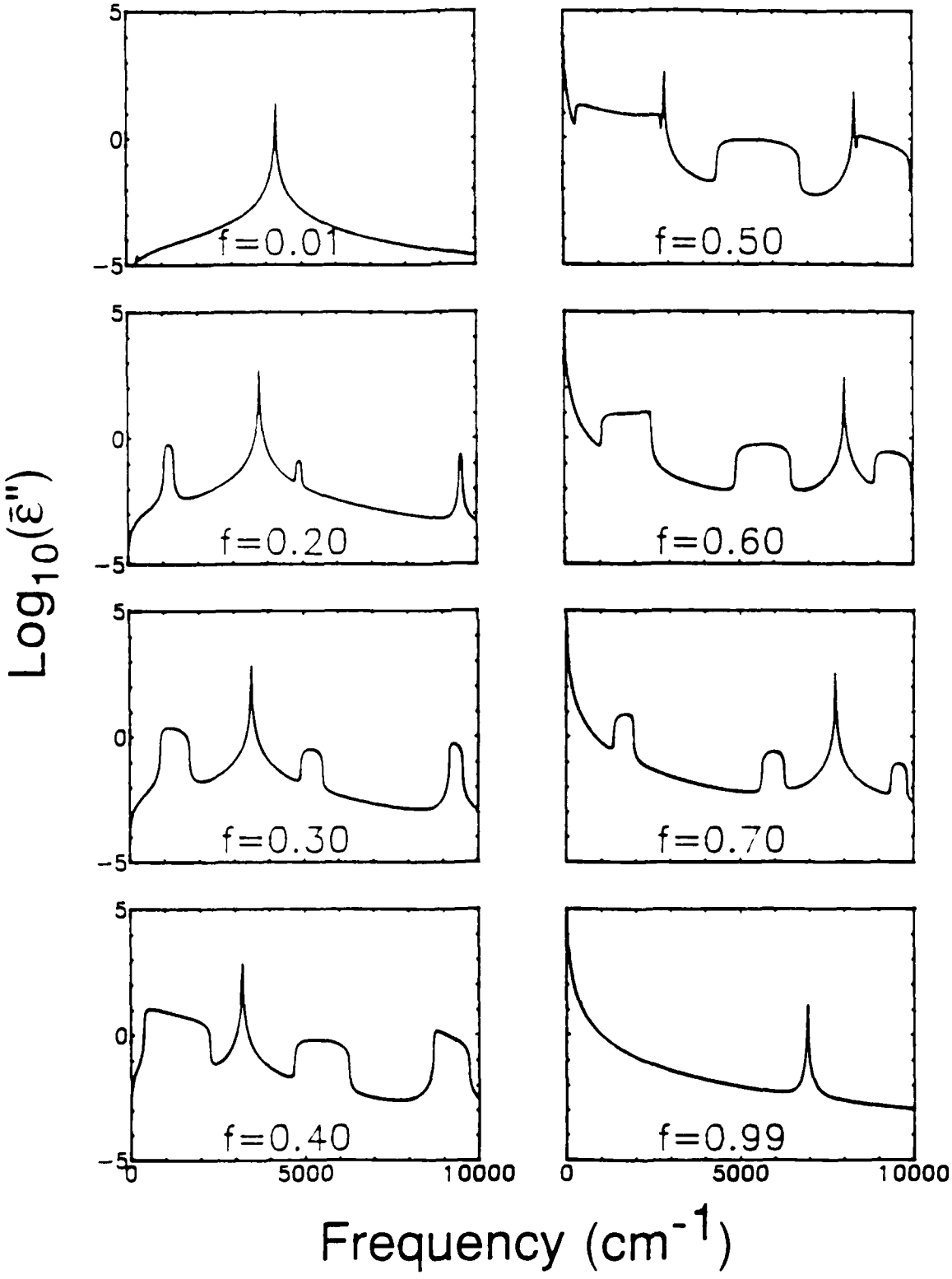

MacMILLAN, DEVATT, + MANTESE FIG. 4

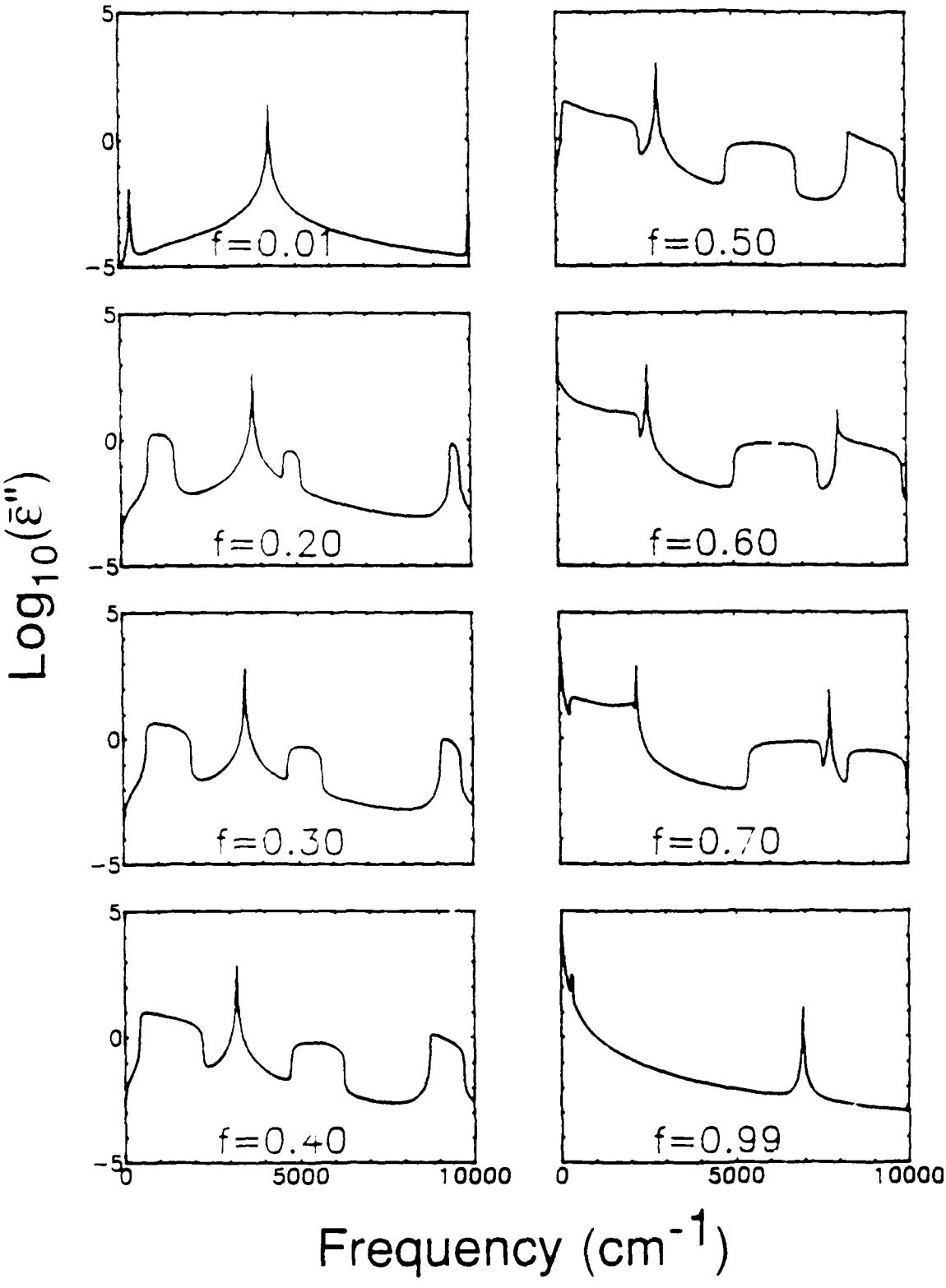

MacMILLAN, DISVATY, & MANTESE FIG. 5

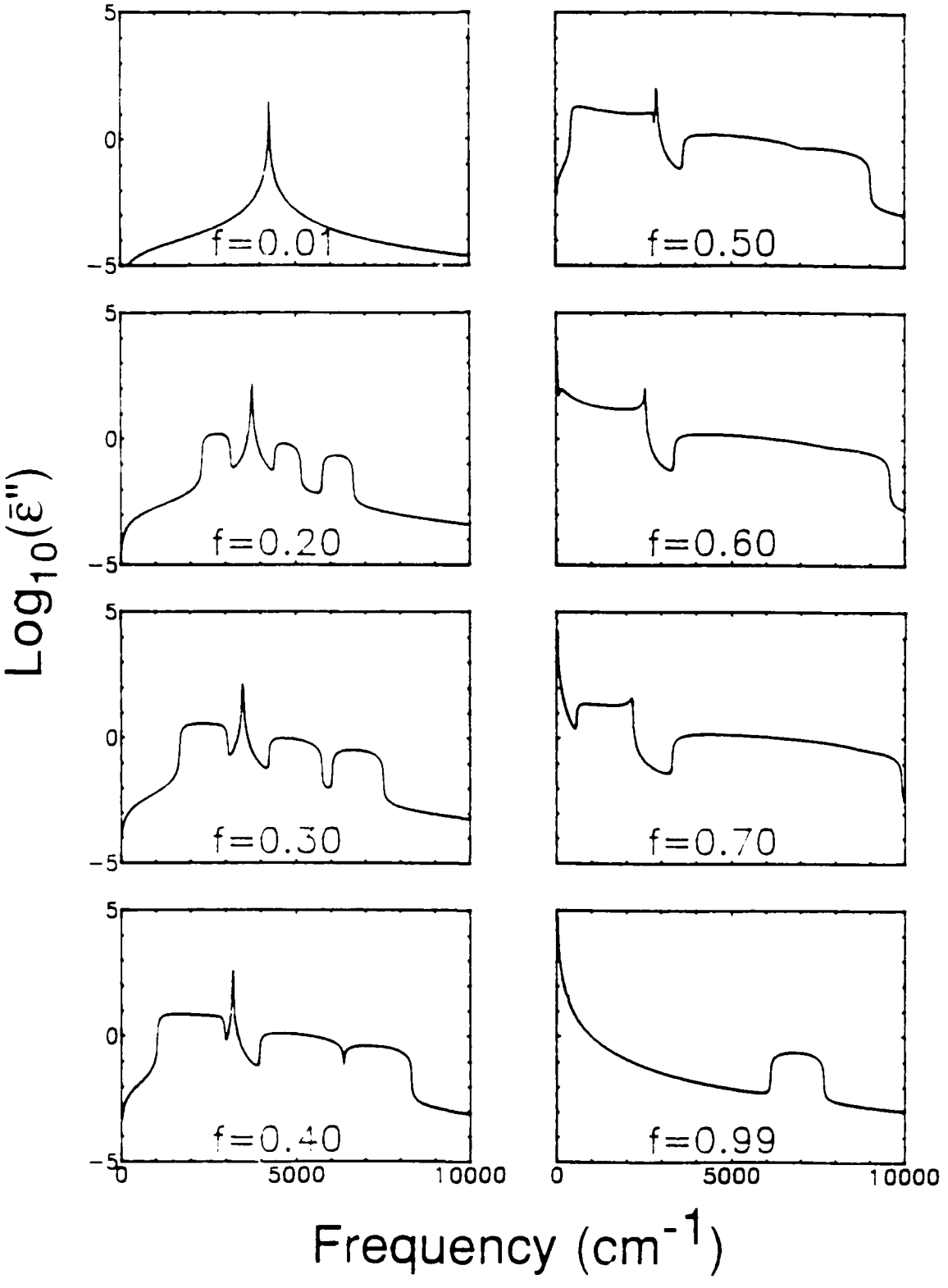

MCC MILLAN, DEVATY, + MANTESE, FIG. 6

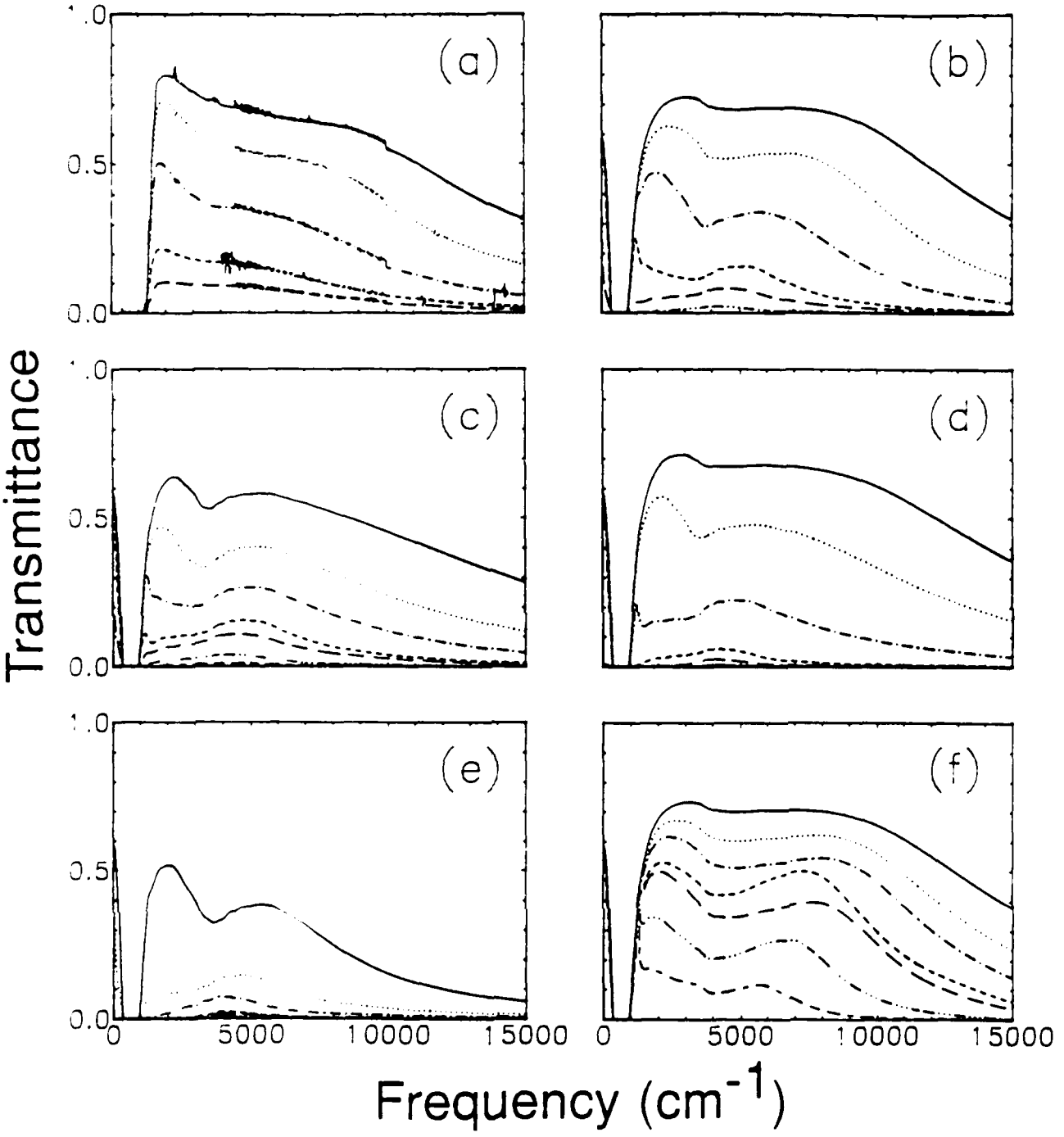

MacMILLAN, DEVATT, + MANTESE FIG. 7

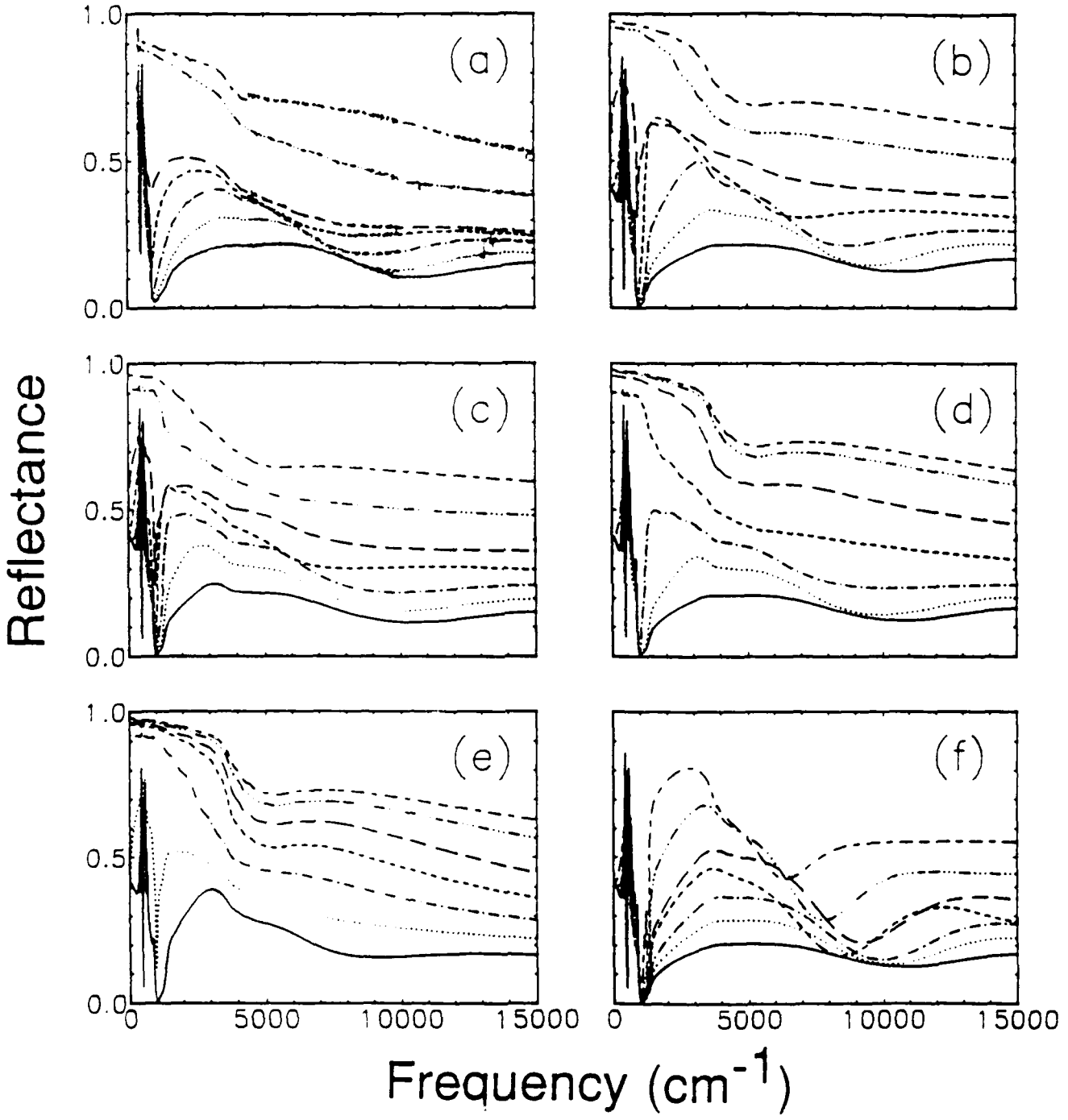

MacMILLAN, DEVATY + MAITISS FIG 2

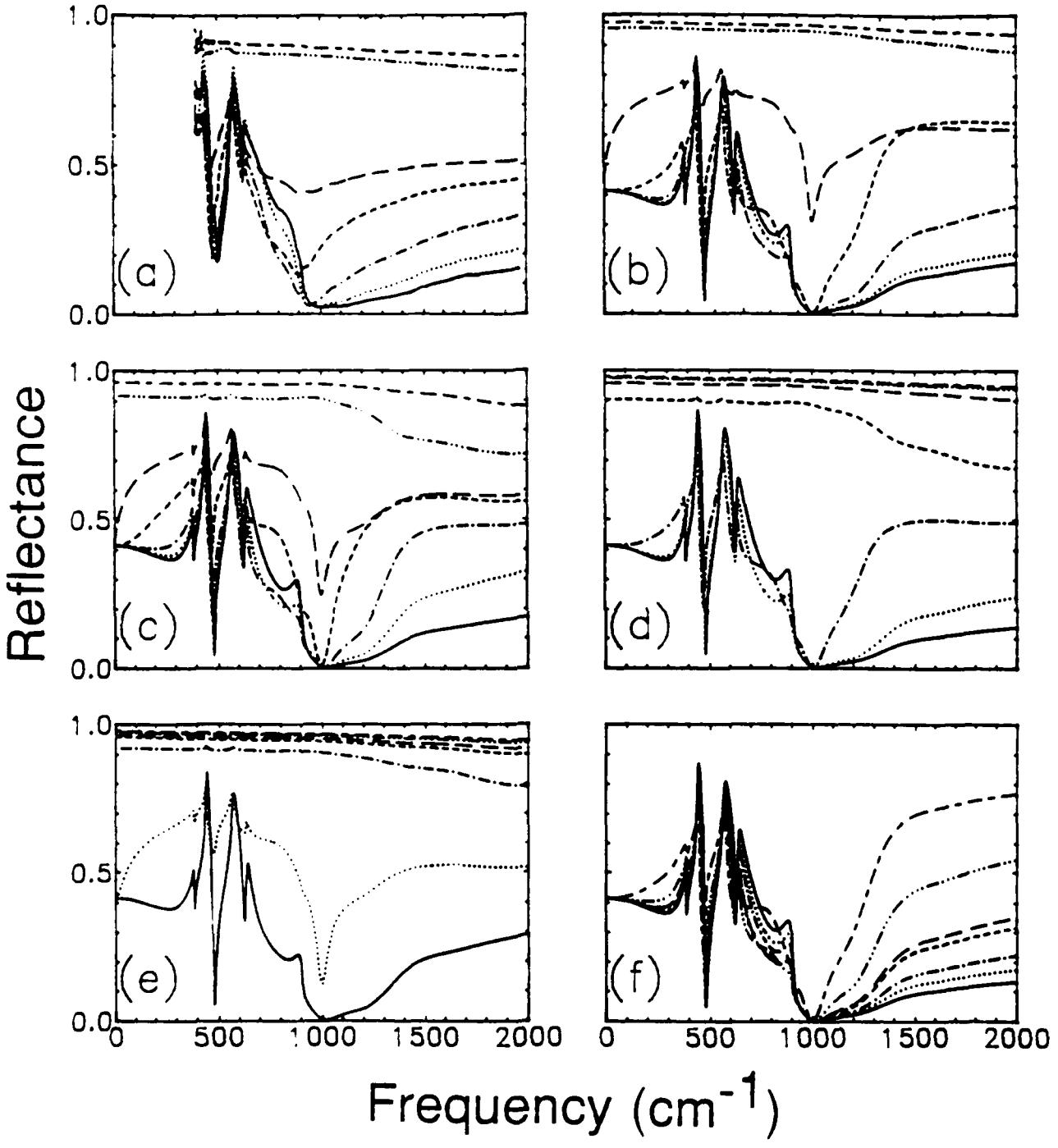

MacMILLAN, DEVATY, + MANTESE FIG. 7

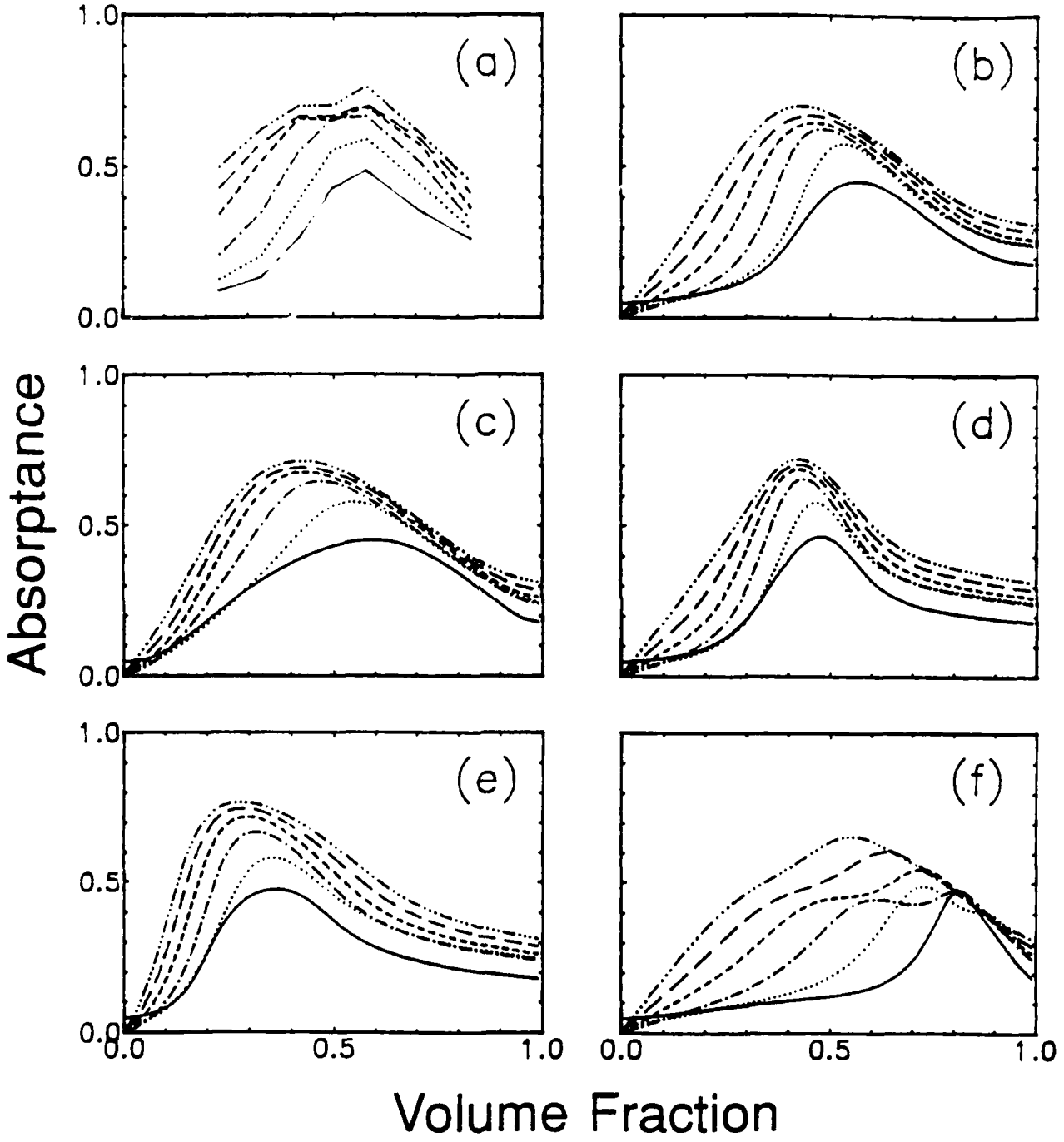

McMillan, Devaty + Mantic Fig. 10